Direct evidence for activity-dependent glucose phosphorylation in neurons with implications for the astrocyte-to-neuron lactate shuttle

Anant B. Patel[a,b,1], James C. K. Lai[c], Golam M. I. Chowdhury[a,d], Fahmeed Hyder[a,e,f], Douglas L. Rothman[a,e,f], Robert G. Shulman[a,1], and Kevin L. Behar[a,d,1]

[a]Magnetic Resonance Research Center and Departments of [e]Diagnostic Radiology, [d]Psychiatry, and [f]Biomedical Engineering, Yale University, New Haven, CT 06520; [c]Department of Biomedical and Pharmaceutical Sciences, College of Pharmacy, Division of Health Sciences, Idaho State University, Pocatello, ID 83209; and [b]NMR Microimaging and Spectroscopy, CSIR-Centre for Cellular and Molecular Biology, Council for Scientific and Industrial Research, Hyderabad 500007, India

Contributed by Robert G. Shulman, February 26, 2014 (sent for review March 13, 2013)

Previous ^{13}C magnetic resonance spectroscopy experiments have shown that over a wide range of neuronal activity, approximately one molecule of glucose is oxidized for every molecule of glutamate released by neurons and recycled through astrocytic glutamine. The measured kinetics were shown to agree with the stoichiometry of a hypothetical astrocyte-to-neuron lactate shuttle model, which predicted negligible functional neuronal uptake of glucose. To test this model, we measured the uptake and phosphorylation of glucose in nerve terminals isolated from rats infused with the glucose analog, 2-fluoro-2-deoxy-D-glucose (FDG) in vivo. The concentrations of phosphorylated FDG (FDG_{6P}), normalized with respect to known neuronal metabolites, were compared in nerve terminals, homogenate, and cortex of anesthetized rats with and without bicuculline-induced seizures. The increase in FDG_{6P} in nerve terminals agreed well with the increase in cortical neuronal glucose oxidation measured previously under the same conditions in vivo, indicating that direct uptake and oxidation of glucose in nerve terminals is substantial under resting and activated conditions. These results suggest that neuronal glucose-derived pyruvate is the major oxidative fuel for activated neurons, not lactate-derived from astrocytes, contradicting predictions of the original astrocyte-to-neuron lactate shuttle model under the range of study conditions.

neuroenergetics | glutamate–glutamine cycle | neuronal glucose phosphorylation | synaptoneurosomes | 2-fluorodeoxyglucose

Metabolic and neurophysiological research has experimentally related brain energy consumption, in the form of glucose oxidation, to the brain work supporting neuronal firing. Carbon-13 magnetic resonance spectroscopy (MRS) measurements (1, 2) of the associated fluxes in cerebral cortex of anesthetized rats over a range of electrical activity revealed, surprisingly, a near 1:1 relationship (in molar equivalent units) between increments in the glutamate–glutamine neurotransmitter cycle and neuronal glucose oxidation. Subsequent studies of rat and human cerebral cortex have been consistent with this finding (3, 4). The near 1:1 flux relation was consistent with a cellular/molecular model, originally proposed by Pellerin and Magistretti (5), and subsequently expanded to include the glutamate/glutamine cycle (1, 6). Evidence for the astrocyte-to-neuron lactate shuttle (ANLS) model is summarized in ref. 7. In this model (Fig. 1*A*), glutamate released from neurons is taken up by astrocytes and converted to glutamine using ATP derived from glycolysis. Lactate produced by this process is transferred to neurons where oxidation occurs. This ANLS model predicts a 1:1 relationship between increments in astrocytic glutamate uptake and glycolysis. Glycolytically derived ATP might provide for more rapid clearance of glutamate from the synaptic cleft into astrocyte processes devoid of mitochondria (8).

The ANLS hypothesis has been challenged on biochemical, in vivo, in situ, and in vitro experimental and theoretical grounds (9–13), as well as the lack of direct in vivo evidence for oxidation of astroglia-derived lactate by neurons. The experimental data against the ANLS model are described in a recent review by Dienel (13). The present study tested predictions of the ANLS model in anesthetized rats (both at baseline and during seizure-induced activation) by direct measurement in brain nerve terminals of the uptake and phosphorylation of an i.v.-infused glucose analog, 2-fluoro-2-deoxy-D-glucose (FDG). To test the hypothesized model (1, 6) (Fig. 1*A*), we measured the rate of glucose phosphorylation in nerve terminals isolated from the brains of rats receiving a short-timed infusion of FDG mixed with ^{13}C-labeled glucose. FDG is phosphorylated by hexokinase to fluoro-2-deoxy-glucose-6-phosphate (FDG_{6P}), which is metabolized only to a limited extent; thus, FDG_{6P} accumulates in neural cells at a rate proportional to glucose utilization (14). The FDG and ^{13}C-glucose mixture (1:7) was infused for 8 min followed by a 52-min washout of FDG by infusing only ^{13}C-glucose (Fig. 2*A*), after which the animals were euthanized and the nerve terminals were isolated. FDG_{6P} was measured in extracts using ^{19}F NMR and normalized to *N*-acetylaspartate (NAA) or glutamate plus γ-aminobutyrate (GABA), predominantly neuronal metabolites, measured in the same extracts using ^{1}H-[^{13}C] NMR. Measurements were made both of nerve terminals and of total brain tissue homogenate, the latter consisting of metabolites from all cells, including neurons and astrocytes. Comparisons were made of the normalized FDG_{6p} formed in brain nerve terminals and homogenate

Significance

A near one-to-one relationship had previously been observed between increments in the fluxes of the glutamate–glutamine neurotransmitter cycle and neuronal glucose oxidation in the tricarboxylic acid (TCA) cycle. This flux relationship was consistent with a hypothesized mechanism involving glycolytic ATP in astrocytes and astrocyte-to-neuron lactate shuttling. Here, 2-fluoro-2-deoxy-D-glucose was used to evaluate the glucose flux through glycolysis and the TCA cycle in nerve terminals isolated from the brains of rats under baseline and high-activity conditions. In a direct contradiction of this hypothesis, the results show that nerve terminals metabolize significant amounts of glucose.

Author contributions: A.B.P., D.L.R., R.G.S., and K.L.B. designed research; A.B.P., J.C.K.L., G.M.I.C., and K.L.B. performed research; A.B.P., J.C.K.L., and K.L.B. analyzed data; A.B.P., F.H., D.L.R., R.G.S., and K.L.B interpreted the data; A.B.P., F.H., D.L.R., R.G.S., and K.L.B. wrote the paper; and K.L.B. supervised and directed the overall project.

The authors declare no conflict of interest.

[1]To whom correspondence may be addressed. E-mail: kevin.behar@yale.edu, robert.shulman@yale.edu, or abpatel@ccmb.res.in.

This article contains supporting information online at www.pnas.org/lookup/suppl/doi:10.1073/pnas.1403576111/-/DCSupplemental.

NEUROSCIENCE

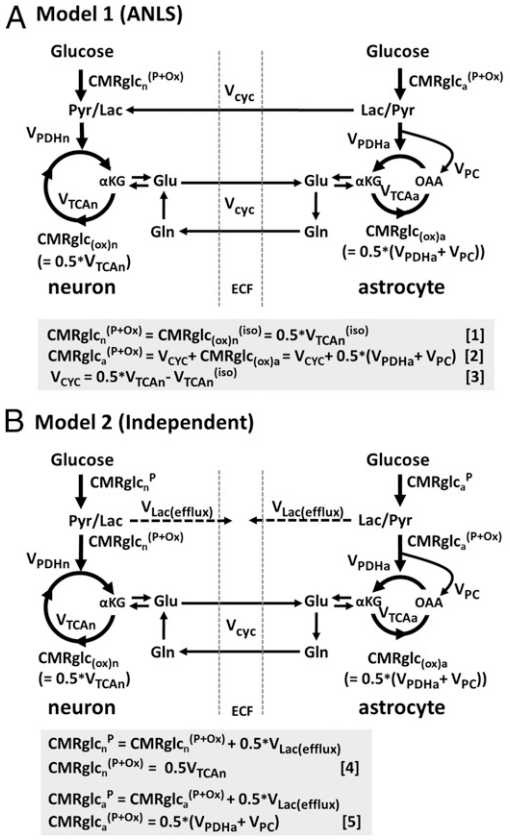

Fig. 1. Schematic depiction of two neuroenergetics models under consideration to account for the 1:1 flux relationship between increments in V_{cyc} and V_{TCAn}. (*A*) ANLS-type model (model 1) described by Sibson et al. (1). Above isoelectricity, lactate transfer from astrocytes to neurons (expressed as glucose equivalents) is determined by the rate of the glutamate–glutamine cycle, V_{cyc}. Neuronal glucose phosphorylation was assumed to be equivalent to the isoelectric rate for all activity levels, i.e., in *A*, $CMRglc_n^{(P+Ox)} = CMRglc_{(ox)n}^{(iso)}$. Predicted rates of $CMRglc_n^{(P+Ox)}$ for model 1 were calculated using Eq. **1**, shown at the bottom of *A*. In the revised description of model 1 by Hyder et al. (3), glucose phosphorylation in neurons above isoelectricity can occur depending on the magnitude of astroglial oxidation and its dependence on neural activity. (*B*) Independent-type model (model 2) in which neurons and astrocytes take up and oxidize glucose according to their respective energy needs. Phosphorylated glucose not oxidized within the cell may be effluxed as lactate, $V_{Lac(efflux)}$, which is shown by dashed lines, reflecting uncertainty of the lactate-releasing neural cells (13, 41). Predicted rates of $CMRglc_n^{(P+Ox)}$ for model 2 were calculated using Eq. **4**, shown at the bottom of *B*. $CMRglc_{(ox)a}$, rate of glucose oxidation in astrocytes $[= 0.5 * (V_{PDHa} + V_{PC})]$; $CMRglc_{(ox)n}^{(iso)}$, rate of glucose oxidized in neurons at isoelectricity $(= 0.5*V_{TCAn}^{(iso)})$; $CMRglc_a^P$, rate of total glucose phosphorylation in astrocytes, which includes oxidative and nonoxidative (net lactate efflux) catabolism; $CMRglc_a^{(P+Ox)}$, rate of glucose phosphorylation in astrocytes with oxidation, includes lactate efflux to neurons at the rate V_{cyc} (model 1) or to extracellular fluid (model 2); $CMRglc_n^P$, rate of total glucose phosphorylation in neurons, which includes oxidative and nonoxidative (lactate efflux) catabolism; $CMRglc_n^{(P+Ox)}$, rate of glucose phosphorylation in neurons with oxidation; Gln, glutamine; Glu, glutamate; Lac, lactate; OAA, oxaloacetate; Pyr, pyruvate; αKG, α-ketoglutarate; V_{PC}, pyruvate carboxylase rate in astrocytes; V_{PDHa}, pyruvate dehydrogenase rate in astrocytes; V_{TCAa}, TCA cycle flux in astrocytes; V_{TCAn}, TCA cycle flux in neurons $(0.5*V_{TCAn} = CMRglc_{(ox)n})$; $V_{TCAn}^{(iso)}$, TCA cycle flux in neurons at isoelectricity.

during control conditions and a more stimulated state (seizure) induced by the $GABA_A$ receptor antagonist, bicuculline. The normalized FDG flux in nerve terminals was then compared with the cortical flux of glucose oxidation, measured in vivo in a previous study of anesthetized rats (15), as well as with the flux in whole brain homogenate, both of which included neuronal and glial contributions. The present results reveal high levels of neuronal phosphorylation of FDG, suggesting that over a significant activity range, neurons are capable of supporting a substantial fraction of their substrate requirements by direct uptake and phosphorylation of glucose.

Results

FDG Metabolism Reflects Premortem Glucose Phosphorylation. FDG levels and enrichments in arterial plasma increased rapidly during the i.v. FDG/[1,6-$^{13}C_2$]glucose infusions in both saline-injected (control) and bicuculline-injected animals, reaching average values of ∼0.8–1.1 mM and ∼7%, respectively (Fig. 2 and Table S1). Cessation of the FDG infusion at 8 min led to declines in plasma FDG levels to <0.2 mM and <2 mol% by 60 min, when animals were euthanized and nerve terminals were isolated (Fig. S1 and Table S1). In pilot experiments conducted without a washout period (euthanasia and terminal isolation at 8 min), blood and brain FDG levels were much higher (Fig. S2) than with washout (Fig. 2 *B* and *C*). Thus, the washout significantly reduced the levels of FDG in blood and brain, ensuring that brain FDG_{6P} accumulation mostly reflects premortem metabolism.

Glucose Phosphorylation Levels Are High in Nerve Terminals. Fig. 2 *B* and *C* depicts ^{1}H-decoupled ^{19}F NMR spectra of nerve terminal and homogenate extracts prepared from control and seizing rats infused with FDG and [1,6-$^{13}C_2$]glucose. The α and β anomers of FDG_{6P} prominently appear in the ^{19}F NMR spectrum. To compare the levels of FDG_{6P} for different nerve terminal preparations, FDG_{6P} was expressed as a ratio with NAA, a neuronal marker, thus normalizing FDG_{6P} to the neuronal fraction. We compared FDG_{6P}/NAA for nerve terminals and the brain homogenate as a measure of glucose phosphorylation in "neurons" to total glucose phosphorylation in brain homogenate. Unexpectedly, FDG_{6P}/NAA in nerve terminals (0.045 ± 0.007) was not significantly different from that in brain homogenate (0.046 ± 0.010) (Table 1). Because brain homogenate includes neurons and astrocytes, prima facie glucose phosphorylation appeared to be dominant in neurons. Similar results were obtained when FDG_{6P} was referenced to the sum of the steady-state concentrations of glutamate-$^{13}C_4$ and GABA-$^{13}C_2$, produced by metabolism of the coinfused [1,6-$^{13}C_2$] glucose, or the sum of glutamate and GABA (Table S2), all predominately neuronal metabolites.

Seizures Increase Nerve Terminal Glucose Phosphorylation. FDG_{6P} was substantially increased in nerve terminals of bicuculline-treated rats compared with saline-injected controls (Fig. 2*B*). In nerve terminals from seizing rats, FDG_{6P}/NAA was 208% of control, comparable to that seen in brain homogenate (189% of control) (Table 1 and Fig. 2*C*). Similar increases were also seen when FDG_{6P} was expressed relative to the sum of ^{13}C-labeled glutamate and GABA (nerve terminals, 188% of control; homogenate, 260% of control) or the sum of their total levels (nerve terminals, 196% of control; homogenate, 220% of control) (Table S2). Thus, increased activity led to a large increase in terminal glucose phophorylation. We also compared the seizure-induced changes in FDG_{6P}/NAA for a small piece of parietal/temporal cortex with cortical glucose consumption ($CMRglc_{(ox)n}$ and $CMRglc_{(tot)}$) reported in a previous in vivo ^{13}C NMR study (15) (Table S3). In the in vivo study, $CMRglc_{(tot)}$ was estimated as the sum of glucose oxidation and the initial rate of lactate accumulation during seizure onset. The seizure-related change in FDG_{6P}/NAA (260% of control) was similar to the change in $CMRglc_{(tot)}$ during seizures (277%) but less than $CMRglc_{(tot)}$ at seizure onset (470%). The larger change in $CMRglc_{(tot)}$ during seizure onset than in FDG_{6P}/NAA could be related to the contribution of glial glycogen breakdown to net lactate formation, which also is the likely source of lactate (and glutamate) isotopic dilution seen during early seizures (15).

Nerve Terminal Astroglial Contamination Is Low. Several glial-associated markers were assessed to estimate glial contamination

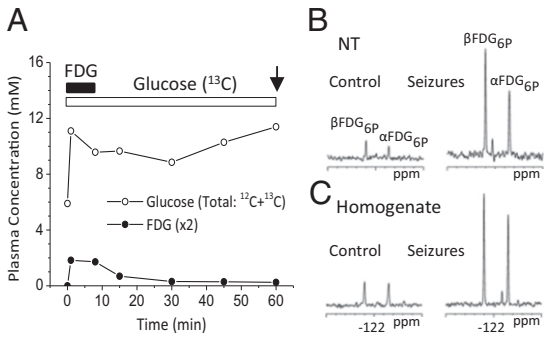

Fig. 2. Time courses of blood FDG and glucose concentrations during FDG/[1,6-$^{13}C_2$] glucose infusion (*A*) and ^{19}F NMR spectra of nerve terminal (NT) (*B*) and homogenate (*C*) extracts for control and seizure conditions. FDG was infused for 8 min (solid bar) and [1,6-$^{13}C_2$] glucose for 60 min (open bar) followed by euthanasia and nerve terminal preparation (arrow). α,βFDG$_{6P}$, 2-fluoro-2-deoxyglucose-6-phosphate; with resolved C1 α and β anomers.

of nerve terminals (Fig. S3). Glutamine, a glial biosynthetic product, was not detected in extracts of nerve terminals, in contrast to cortex or whole brain homogenate where prominent signals of glutamine were observed (Fig. S4). Formation of ^{13}C-labeled glutamine, which was seen in homogenates incubated in vitro with [2-^{13}C]acetate (a glial substrate), or [1,6-$^{13}C_2$]glucose plus [U-$^{13}C_5$]glutamate (neuronal and glial substrates), was not detected during incubations with freshly isolated nerve terminals, although both led to substantial glutamate ^{13}C labeling as expected for nerve terminals (Fig. S3 *B* and *C*). Because gliosomes would be expected to have an abundance of glutamate and glucose transporters, as well as glycolytic and tricarboxylic acid (TCA) cycle enzymes capable of metabolizing [U-$^{13}C_5$]glutamate to [U-$^{13}C_5$]glutamine and [1,6-$^{13}C_2$]glucose to [4-^{13}C]glutamate/[4-^{13}C]glutamine, respectively, we combined both ^{13}C-labeled substrates to isotopically enrich multiple pathways leading to glial glutamine synthesis, reducing potential dilution inflows and increasing assay sensitivity to reveal glial metabolism. Glutamine synthetase activity measured in nerve terminals was 3.3% of total homogenate (Fig. S3*A*). Immunoblots against glial-expressed GFAP established an upper limit of contamination by glia or glial fragments of ~9–17% of total protein (Fig. S3*D*). Together, the results strongly suggest a relatively low level of gliosome contamination of the nerve terminals.

Predictions of Two Neuroenergetics Models. The support of the ANLS model (Fig. 1*A*, model 1) by the incremental 1:1 experimental relationship was based on the hypothesis that glycolytic ATP supports glutamate uptake and conversion to glutamine in astrocytes; one molecule of ATP would be expended by Na^+/K^+-ATPase to expel the three Na^+ ions cotransported with each molecule of glutamate, and another to convert glutamate to glutamine by glutamine synthetase. If this process is performed in astrocytes using glycolytic ATP, it leads to a 1:1 relationship between the glutamate–glutamine cycle and astrocytic glucose uptake with subsequent oxidation in the neuron after lactate shuttling (1, 6). The faster synthesis of ATP by glycolysis over oxidative phosphorylation would promote faster clearance of glutamate from the extracellular space, which occurs within ~10 ms (16), providing a mechanistic rationale in support of the ANLS model. Despite considerable scientific debate, direct experimental evidence for or against the ANLS model as the source of the 1:1 relationship between ΔV_{cyc} and $\Delta CMRglc_{(ox)n}$ is lacking. Direct evidence was sought in this study by comparing the amount of the glucose analog (FDG) accumulated by neurons and glia under different levels of brain activity with model predictions. For the model shown in Fig. 1*A*, equations were derived for the rates of glucose phosphorylation in neurons and astrocytes followed by complete oxidation ($CMRglc_{n,a}^{(P+Ox)}$) under the constraint that astroglial glutamate uptake and conversion to glutamine is coupled to astrocytic glucose uptake in a 1:1 relation.

Table 1. Ratio of FDG$_{6P}$-to-NAA in nerve terminals and brain homogenate under control and seizure conditions

	FDG$_{6P}$/NAA		
	Control (Con)	Seizure (Sez)	Ratio (Sez/Con)
Nerve terminals	0.045 (0.007)	0.093 (0.015)	2.08 (0.49)
Homogenate	0.046 (0.010)	0.086 (0.012)	1.89 (0.51)

Ratios reflect mean (± SD) of three separate preparations each.

$$\textbf{Model 1 (ANLS)}\ \textit{neurons}:\quad CMRglc_n^{(P+Ox)} = 0.5V_{TCAn}^{(iso)}, \qquad [1]$$

$$\textit{astrocytes}:\quad CMRglc_a^{(P+Ox)} = V_{cyc} + 0.5(V_{PDHa} + V_{PC}), \qquad [2]$$

$$V_{cyc} = 0.5V_{TCAn} - 0.5V_{TCAn}^{(iso)}, \qquad [3]$$

where V_{TCAn} is neuronal TCA cycle flux, $V_{TCAn}^{(iso)}$ is neuronal TCA cycle flux under isoelectric (nonsignaling) conditions, V_{PDHa} is astroglial pyruvate dehydrogenase flux, and V_{PC} is astroglial pyruvate carboxylase flux (not present in the neurons). The factor of 0.5 refers to the two molecules of pyruvate/lactate formed per molecule of glucose metabolized by glycolysis, which enters the TCA cycle via pyruvate dehydrogenase (neurons and astrocytes) or pyruvate carboxylase (astrocytes). We note that glucose derived from glycogen hydrolysis in astrocytes bypasses hexokinase and is not included in $CMRglc_a^P$.

The predictions of an alternative to the ANLS-based model (Fig. 1*B*, model 2), in which neurons and astrocytes phosphorylate glucose independently according to their energy needs, were also tested by the present data; in this model, the 1:1 flux relationship between ΔV_{cyc} and $\Delta CMRglc_{(ox)n}$ (or equivalently, $\Delta 0.5V_{TCAn}$) arises in neurons rather than astrocytes. This scenario would be consistent with evidence from studies of cultured astrocytes that plasma membrane ATPase uses ATP derived by glycolysis or oxidative phosphorylation equally well (17), and that ATP generated by both pathways support glutamate uptake (18).

$$\textbf{Model 2 (indep.)}:\ \textit{neurons}:\quad CMRglc_n^{(P+Ox)} = 0.5V_{TCAn}, \qquad [4]$$

$$\textit{astrocytes}:\quad CMRglc_a^{(P+Ox)} = 0.5(V_{PDHa} + V_{PC}). \qquad [5]$$

Comparison with Results. Table 2 presents the values predicted by the two models of $CMRglc_n^{(P+Ox)}$ and total glucose oxidation ($CMRglc_{(ox)n+a}$) under control and seizure conditions, along with their respective seizure-to-control (Sez/Con) ratios. These values were calculated from the equations in *Predictions of Two Neuroenergetics Models* using previously reported rates of neuronal and astroglial glucose oxidation and glutamate/glutamine cycling measured under similar conditions, as input. These predictions were compared with the measured FDG$_{6P}$/NAA (from Table 1) for the isolated nerve terminals (assumed to represent the neuronal pool) relative to FDG$_{6P}$/NAA for whole brain homogenate, the latter taken to represent whole brain glucose phosphorylation. Likewise, the relations describing the predicted relative change (Sez/Con) in FDG$_{6P}$/NAA are:

$$\textbf{Model 1 (ANLS):}\ (FDG_{6P}/NAA)_{Sez}\Big/(FDG_{6P}/NAA)_{Con} = \left(0.5V_{TCAn}^{(iso)}\right)_{Sez}\Big/\left(0.5V_{TCAn}^{(iso)}\right)_{Con} = 1, \quad [6]$$

$$\textbf{Model 2 (indep.):}\ (FDG_{6P}/NAA)_{Sez}\Big/(FDG_{6P}/NAA)_{Con} = (0.5V_{TCAn})_{Sez}\Big/(0.5V_{TCAn})_{Con}. \quad [7]$$

The predicted change in FDG_{6P}/NAA for total brain homogenate was calculated as the sum of neuronal and astrocytic glucose oxidation (Table 2), $(CMRglc_{(ox)n+a})_{Sez}/(CMRglc_{(ox)n+a})_{Con}$. Fig. 3 compares measured and predicted ratios of the two models. This analysis, being the more direct test, compares incremental total and neuronal glucose phosphorylation between control and seizure conditions. As seen in Fig. 3, the experimentally determined ratio is substantially closer to model 2 (independent) than model 1 (ANLS), and similar to brain homogenate.

Discussion

Factors Influencing the FDG_{6P}/NAA Ratio in Nerve Terminals. ***NAA as a measure of neuronal cytosolic volume.*** The conclusion that similar amounts of FDG were taken up (on a per cellular cytosol basis) in the nerve terminals and in total neuronal volume assumes that NAA, which is found exclusively in neurons, reflects quantitatively the neuronal cytosolic volume. The concentration of NAA is relatively homogenous (6–8 mM) across multiple rat brain regions (19). Because the rate of intracellular diffusion of NAA greatly exceeds its metabolic turnover, the intraneuronal distribution of NAA is anticipated to be relatively homogenous. For example, based on the apparent diffusion coefficient of NAA of 0.27 μm^2/ms determined by MRS (20), mixing of NAA throughout neurons would occur in ∼60 min, whereas the metabolic turnover of NAA is slow [NAA_{C3} time constant, 13–14 h (21)].

Accuracy with which nerve terminals reflect total neuronal FDG uptake. Surprisingly, the absolute FDG_{6P}/NAA ratio for the nerve terminals was the same as that for total brain homogenate, which contains contributions of glucose uptake from astroglia and other neural cells not containing NAA. A ∼20–30% higher FDG_{6P}/NAA would be anticipated for brain homogenate based on estimates of the rate of glial glucose oxidation (3, 22, 23). A possible explanation for this discrepancy is that FDG_{6P} could be more concentrated in nerve terminals. Evidence for this was previously reported (24, 25) using ^{14}C-2-deoxyglucose autoradiography. Based on considerations of energy budget modeling and mitochondrial density (26), and in vitro measurements (27), the highest neuronal rates of glucose uptake and oxidation may occur in postsynaptic dendrites, spines, and axon collaterals. Thus, differences in the distribution of FDG_{6P} between presynaptic and postsynaptic neuronal elements may explain the equal FDG_{6P}/NAA ratios found.

Effect of postmortem anaerobic glycolysis. Another factor that could lead to an artifactually high amount of FDG_{6P} in the nerve terminals would be extensive postmortem anaerobic glycolysis. To minimize this possibility, we designed the FDG infusion so that the maximum FDG uptake would occur during the premortem stage by incorporating a washout period of 52 min. At the end of the washout period, the mole fraction of FDG to glucose in blood was reduced to <2% (Table S1 and Fig. S1), which would insignificantly impact the FDG_{6P} levels.

Effects of FDG on energetics, kinetics, and metabolism beyond FDG_{6P}. FDG competes with glucose for transport into the brain and, at high doses, can interfere with ATP formation by limiting glucose availability and sequestering inorganic phosphate (P_i) as FDG_{6P}. The average FDG_{6P} concentrations, 0.44 $\mu mol \cdot g^{-1}$ (control) and 1.1 $\mu mol \cdot g^{-1}$ (seizure) in cortex and 4.2 $nmol \cdot mg^{-1}$ protein (control) and 19.9 $nmol \cdot mg^{-1}$ protein (seizures) in the nerve terminals, were significantly less than those reported in two previous in vivo studies using bolus i.v. or intra-arterial injections (500 mg/kg) of 2-[6-^{13}C]deoxyglucose (28) or 2-deoxyglucose (29). Deuel et al. (29) observed no significant effects of the FDG infusion on brain levels of ATP, phosphocreatine, or P_i, or in the intracerebral pH as measured by ^{31}P MRS, despite using approximately a 10× higher dose of FDG than in the present study. The relatively low brain FDG_{6P} concentration was also reflected in the absence of other fluorinated phosphorylated metabolites of FDG (27). However, low levels of fluorodeoxymannose-6-P (β, −59.15 ppm; α, −40.85) were detected in the homogenate extract, which may reflect postmortem metabolism. Thus, FDG and FDG_{6P} levels would not be expected to significantly impact glucose metabolism.

A potential source of overestimation of nerve terminal glucose uptake in the seizure condition is that the lumped constant (LC), which corrects for different kinetic properties of FDG versus glucose, may rise steeply when brain glucose concentration falls to <1 $\mu mol \cdot g^{-1}$ (12). In awake rats during 1 h of bicuculline seizures (30), glucose levels remained above the critical value of ∼1 $\mu mol \cdot g^{-1}$, supporting our use of a single LC value. However, if the decline in glucose is more pronounced in the nerve terminals compared with whole tissue, FDG/glucose ratio would rise, leading to artifactually high rates of FDG phosphorylation relative to glucose. A study of glucose utilization using [2-^{14}C]deoxyglucose (DG) during penicillin-induced seizures (31) found that brain glucose decreased by 20% (to 1.7 $\mu mol \cdot g^{-1}$), which corresponded to an increase in LC (and overestimate of CMRglc rate) of ∼10%. Because FDG is transported and phosphorylated faster than

Table 2. Predicted change in rates of neuronal glucose phosphorylation for two neuroenergetics models

	Control (Con)		Seizure (Sez)		Ratio (Sez/Con)	
	$CMRglc_n^{(P+Ox)}$	$CMRglc_{(ox)n+a}$	$CMRglc_n^{(P+Ox)}$	$CMRglc_{(ox)n+a}$	$CMRglc_n^{(P+Ox)}$	$CMRglc_{(ox)n+a}$
Model 1 (ANLS)	0.08 (0.02)	0.44 (0.05)	0.08	0.79 (0.14)	1.0	1.8 (0.26)
Model 2 (Indep.)	0.26 (0.05)	0.44 (0.05)	0.57 (0.14)	0.79 (0.14)	2.2 (0.67)	1.8 (0.26)

Values reflect mean (± SD). $CMRglc_n^{(P+Ox)}$ is the rate of glucose phosphorylation in neurons followed by complete oxidation in the neuronal TCA cycle and calculated using values of $V_{TCAn}^{(iso)}$ and V_{TCAn} according to Eqs. **1** and **4** describing the two energetics models (Fig.1). $CMRglc_{(n\ or\ a)}^{(P+Ox)}$ will be less than total glucose phosphorylation in neurons or astrocytes ($CMRglc_{(n\ or\ a)}^{P}$) to the extent that net lactate is formed and effluxed, which is depicted in model 2 (Fig. 1*B*) by the dashed arrow. $CMRglc_{(ox)n+a}$ is the rate of total glucose oxidation occurring in neurons plus astrocytes (= $CMRglc_{(ox)n} + CMRglc_{(ox)a}$), where $CMRglc_{(ox)n} = 0.5V_{TCAn}$ and $CMRglc_{(ox)a} = 0.5(V_{PC} + V_{PDHa})$. Values used in the calculations: $0.5V_{TCAn}^{(iso)} = 0.08(\pm 0.02)$ $\mu mol \cdot g^{-1} \cdot min^{-1}$ (1, 15); $CMRglc_{(ox)n} = 0.26(\pm 0.05)$ (control) and $0.57(\pm 0.14)$ $\mu mol \cdot g^{-1} \cdot min^{-1}$ (seizure) (15); $CMRglc_{(ox)a}$ and $CMRglc_{(ox)a}^{(iso)}$ were estimated from the respective slope and *y* intercept of the relation ($CMRglc_{(ox)a} = 0.11V_{cyc} + 0.16$) obtained by a linear least-squares fit to a plot of $CMRglc_{(ox)a}$ vs. V_{cyc} using values of V_g, V_{PC}, and V_{NT} (=V_{cyc}) for low and moderate activity (34, 35), and of V_g (22), V_{PC} (55), and V_{cyc} (15) for the seizure condition, where $CMRglc_{(ox)a} = V_g/2 + V_{PC}$. Estimated values of $CMRglc_{(ox)a}$ were calculated from this equation giving 0.18 (±0.06) (control) and 0.22 (±0.12) $\mu mol \cdot g^{-1} \cdot min^{-1}$ (seizure) for $V_{cyc} = 0.22$ (±0.08) and 0.52 (±0.06) $\mu mol \cdot g^{-1} \cdot min^{-1}$ (15), respectively. $CMRglc_{(ox)n+a} = CMRglc_{(ox)n} + CMRglc_{(ox)a} = 0.26 + 0.18 = 0.44(\pm 0.05)$ (control) and $0.57 + 0.22 = 0.79$ (±0.14) $\mu mol \cdot g^{-1} \cdot min^{-1}$ (seizure). Expressions relating $CMRglc_{(ox)a}$ to V_{PDHa}, V_g and V_{PC} are found in *SI Text, Effects of Astroglial Glucose Oxidation on Predicted Neuronal Glucose Uptake*.

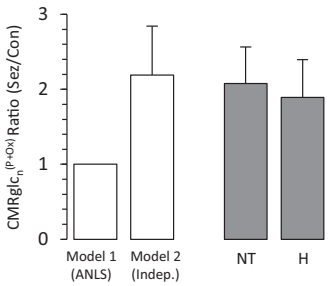

Fig. 3. Comparison of seizure-to-control (Sez/Con) ratios for glucose phosphorylation in nerve terminals (NT) and brain homogenate (H) with predictions of the two neuroenergetics models. Values shown for NT and H reflect the Sez/Con ratios of FDG_{6P}/NAA expressed as mean ± SD (n = 3,3). Predicted rates of neuronal glucose phosphorylation with oxidation, $CMRglc_n^{(P+Ox)}$, were calculated using Eqs. **1**–**3** (model 1) and Eqs. **4** and **5** (model 2) for control and seizure conditions and expressed as a ratio.

2-DG (LC of 0.71 vs. 0.48) (32), the expected overestimate would be lower, ∼5–7%.

Effect of astroglial contamination in the nerve terminal fraction. Another potential source of FDG_{6P} could arise through contamination of nerve terminals by glial processes or gliosomes (33). The nerve terminals were judged to be relatively pure based on the absence of glutamine (a glial marker), their inability to synthesize ^{13}C labeled glutamine from [U-$^{13}C_5$]glutamate and [1,6-$^{13}C_2$]glucose or [2-^{13}C]acetate in vitro when supplied with these substrates, and relatively low enzymatic activity of glutamine synthetase and a glial marker protein (GFAP) (Fig. S3).

Impact of Activity-Dependent Astroglial Glucose Oxidation. In model 1, the glia are approximated as transferring all of the lactate they produce through glycolysis-coupled glutamate uptake to the neuron. However, as discussed in ref. 3, because the astroglia can in principle oxidize the pyruvate resulting from this process, the net transfer of lactate to the neurons may be favored only when the rate of glutamate/glutamine cycling (V_{cyc}) exceeds the rate of astroglial glucose (pyruvate) oxidation. The magnitude of this effect was estimated by combining our previous data on neuronal glucose oxidation and glutamate cycling under similar conditions of halothane anesthesia and seizures (15) with the reported rates of astroglial glucose oxidation (22, 34, 35). Assuming a glial oxidative activity dependence similar to what has been reported in other conditions (22, 23, 36), and the model proposed in ref. 3, the predicted neuronal FDG uptake during seizures compared with control would rise by at most ∼38%, leading to a predicted seizure-to-control ratio of 1.4 rather than 1 (*SI Text*, *Effects of Astroglial Glucose Oxidation on Predicted Neuronal Glucose Uptake*), which still does not agree with the high neuronal uptake of FDG observed.

Potential Neuronal Basis of the 1:1 Ratio. The finding of a large fraction of activity-dependent glucose uptake in neurons requires an alternative explanation of the 1:1 relationship. Two alternate mechanisms have been postulated, one involving the coupling of neuronal glycolysis (or glycolytic ATP) to vesicular loading of glutamate (37, 38) and another involving the coupling of neuronal glutamate formed from glutamine to redox movements into mitochondria via the malate aspartate shuttle (39, 40). Glutamate accumulation into synaptic vesicles is driven by a H^+ electrochemical gradient produced by a vacuolar (H^+)-ATPase, the energetic cost of which was estimated to be ∼0.33 ATP/glutamate (26). Assuming this ATP to be derived entirely from glycolysis would lead to a predicted flux ratio ΔV_{cyc}:$\Delta CMRglc_n^{(P+Ox)}$ of ∼6:1, well above the observed value of 1:1. In the scheme of Hertz and coworkers (39, 40), the processing of glutamine to transmitter glutamate is indirect, involving mitochondrial formation of α-ketoglutarate from glutamine and with efflux to cytoplasm in exchange with malate. Because there is a fixed stoichiometric relationship between the formation of glycolytically produced NADH from glucose and the transfer of reducing equivalents into mitochondria via malate (1 glucose: 2 NADH: 2 malate), the formation of transmitter glutamate from glutamine will correlate with the exchange-mediated flow of glycolytically produced reducing equivalents from cytoplasm to mitochondria. Because one molecule of glucose provides 2 molecules of NADH in cell cytoplasm by glycolysis, the expected incremental glutamine/glucose flux ratio (ΔV_{cyc}:$\Delta CMRglc_n$) would be 2:1 in the compartment of glutamate transmitter synthesis, i.e., the nerve terminal. This value, however, is twice the value of 1:1 determined in vivo. Noting that the measured value of neuronal TCA cycle flux (denominator in the ratio) includes all neuronal compartments, including those where glutamine metabolism and cycling may be limited, e.g., postsynaptic dendritic sites and/or cell bodies, might explain this discrepancy. Rates of glucose oxidation in glutamatergic postsynaptic/dendritic compartments might be expected to be strongly correlated with presynaptic glutamate release and cycling (V_{cyc}), consistent with recent experimental (41) and theoretical findings (27).

Reconciling the Experimental Evidence: Rest vs. Activation. The finding of high resting neuronal FDG phosphorylation in adult rats is consistent with in vivo findings from high-resolution 2-DG autoradiography (42), reporting approximately equal amounts of glucose utilization by neurons and astrocytes. In addition, an in vivo study using the fluorescent glucose analog, 2-deoxy-*N*-(7-nitrobenz-2-oxa-1,3-diazol-4-yl)-aminoglucose (2-NBDG), which is phosphorylated by hexokinase to $2\text{-}NBDP_{6P}$ (43), also found uptake/metabolism in both neurons (hippocampal pyramidal and cerebellar Purkinje cells) and astroglia of adult rats. The in vivo findings, however, are at odds with two recent in vitro studies using 2-NBDG in immature (P10 to P21) cerebellar (44) and hippocampal (45) brain slices, which found less uptake in neurons than in astrocytes, inferring support for the ANLS mechanism. However, the relevance for functional metabolism is problematic because rates of neuronal glucose oxidation and glutamate–glutamine cycling in P10 neocortex are ∼1/3 of the mature cortex (46), and in unstimulated slices, glutamate–glutamine cycling is not detected and oxygen consumption rate is very low (47). Because the quantitative use of 2-NBDG (unlike 2-DG and 2-FDG) and stability of $2\text{-}NBDG_{6P}$ remains to be thoroughly validated (13), conclusions of cell type-specific glucose utilization (and inferences to unmeasured lactate movements) may be premature. Our results go further than previous studies in showing that with intense activation, glucose phosphorylation is increased in nerve terminals, suggesting that direct glucose uptake and oxidation is a major pathway to satisfy energy demands. As such, our findings do not support the proposal that neuronal glycolysis is inhibited under high-activity conditions (48) or that neurons in vivo lack the ability to increase glycolysis as seen in cultured cells (49). However, our results do not rule out an important role for an ANLS mechanism under certain conditions, e.g., that existing during the initial stages of intense neural activation when net glycogen breakdown occurs (50, 51)), such as for seizure onset (15). Also, our findings do not address whether neurons are a source (10, 52) or a sink (5, 53) of the extracellular lactate rise seen with neural activation (see ref. 13 for a review of the evidence on this topic).

Conclusions

The present findings, which indicate that neuronal glycolysis is capable of substantial support of its oxidative needs, are incompatible with an ANLS-type model previously proposed to explain the ∼1:1 relationship observed between ΔV_{cyc} and $\Delta CMRglc_{(ox)n}$, suggesting this relation may arise in neurons. Furthermore, the results demonstrate up-regulation of neuronal glycolysis during neural activation and direct neuronal oxidation of glucose-derived pyruvate; but they do not support astrocytic lactate production strongly coupled with lactate shuttling to neurons to provide a major neuronal fuel. The synaptosome data are consistent with and extend (i.e., by doing the activation in

vivo instead of in vitro) studies of synaptosomes from adult rodents, clearly demonstrating their high capacity for increasing glycolysis and oxidative metabolism.

Materials and Methods

Adult male Wister rats were prepared under halothane anesthesia (15) in accordance with protocols approved by the Yale Animal Care and Use Committee.

FDG and [1,6-$^{13}C_2$]glucose were infused for 8 min, followed by [1,6-$^{13}C_2$]glucose alone (washout) for 60 min.

Nerve terminals were prepared from rat forebrain using isotonic media and Ficoll density gradient centrifugation (54).

Tissue extracts were prepared using ethanol (15) for high-resolution ^{19}F or ^{1}H-[^{13}C] NMR at 11.7T.

The values reported reflect mean ± SD. Statistical significance of differences was assessed by Student *t* test with level of $P < 0.05$. Further details appear in *SI Text*.

ACKNOWLEDGMENTS. The authors thank Bei Wang for animal preparation and Shirley Wang for immunoblotting. This study was supported by National Institutes of Health Grants R01-DK27121 and R01-DK27121-28S.

1. Sibson NR, et al. (1998) Stoichiometric coupling of brain glucose metabolism and glutamatergic neuronal activity. *Proc Natl Acad Sci USA* 95(1):316–321.
2. Shen J, et al. (1999) Determination of the rate of the glutamate/glutamine cycle in the human brain by in vivo ^{13}C NMR. *Proc Natl Acad Sci USA* 96(14):8235–8240.
3. Hyder F, et al. (2006) Neuronal-glial glucose oxidation and glutamatergic-GABAergic function. *J Cereb Blood Flow Metab* 26(7):865–877.
4. Rothman DL, De Feyter HM, de Graaf RA, Mason GF, Behar KL (2011) ^{13}C MRS studies of neuroenergetics and neurotransmitter cycling in humans. *NMR Biomed* 24(8): 943–957.
5. Pellerin L, Magistretti PJ (1994) Glutamate uptake into astrocytes stimulates aerobic glycolysis: A mechanism coupling neuronal activity to glucose utilization. *Proc Natl Acad Sci USA* 91(22):10625–10629.
6. Magistretti PJ, Pellerin L, Rothman DL, Shulman RG (1999) Energy on demand. *Science* 283(5401):496–497.
7. Pellerin L, Magistretti PJ (2012) Sweet sixteen for ANLS. *J Cereb Blood Flow Metab* 32(7):1152–1166.
8. Shulman RG, Hyder F, Rothman DL (2001) Cerebral energetics and the glycogen shunt: Neurochemical basis of functional imaging. *Proc Natl Acad Sci USA* 98(11):6417–6422.
9. Gjedde A, Marrett S (2001) Glycolysis in neurons, not astrocytes, delays oxidative metabolism of human visual cortex during sustained checkerboard stimulation in vivo. *J Cereb Blood Flow Metab* 21(12):1384–1392.
10. Chih CP, Roberts EL, Jr. (2003) Energy substrates for neurons during neural activity: A critical review of the astrocyte-neuron lactate shuttle hypothesis. *J Cereb Blood Flow Metab* 23(11):1263–1281.
11. Hertz L (2004) The astrocyte-neuron lactate shuttle: A challenge of a challenge. *J Cereb Blood Flow Metab* 24(11):1241–1248.
12. Dienel GA (2012) Fueling and imaging brain activation. *ASN Neuro* 4(5):e00093.
13. Dienel GA (2012) Brain lactate metabolism: The discoveries and the controversies. *J Cereb Blood Flow Metab* 32(7):1107–1138.
14. Sokoloff L, et al. (1977) The [^{14}C]deoxyglucose method for the measurement of local cerebral glucose utilization: Theory, procedure, and normal values in the conscious and anesthetized albino rat. *J Neurochem* 28(5):897–916.
15. Patel AB, et al. (2004) Glutamatergic neurotransmission and neuronal glucose oxidation are coupled during intense neuronal activation. *J Cereb Blood Flow Metab* 24(9):972–985.
16. Bergles DE, Diamond JS, Jahr CE (1999) Clearance of glutamate inside the synapse and beyond. *Curr Opin Neurobiol* 9(3):293–298.
17. Silver IA, Erecińska M (1997) Energetic demands of the Na^+/K^+ ATPase in mammalian astrocytes. *Glia* 21(1):35–45.
18. Swanson RA, Benington JH (1996) Astrocyte glucose metabolism under normal and pathological conditions in vitro. *Dev Neurosci* 18(5-6):515–521.
19. Wang J, et al. (2010) Regional metabolite levels and turnover in the awake rat brain under the influence of nicotine. *J Neurochem* 113(6):1447–1458.
20. Pfeuffer J, Tkác I, Gruetter R (2000) Extracellular-intracellular distribution of glucose and lactate in the rat brain assessed noninvasively by diffusion-weighted ^{1}H nuclear magnetic resonance spectroscopy in vivo. *J Cereb Blood Flow Metab* 20(4): 736–746.
21. Choi IY, Gruetter R (2004) Dynamic or inert metabolism? Turnover of N-acetyl aspartate and glutathione from D-[1-^{13}C]glucose in the rat brain in vivo. *J Neurochem* 91(4):778–787.
22. Oz G, et al. (2004) Neuroglial metabolism in the awake rat brain: CO_2 fixation increases with brain activity. *J Neurosci* 24(50):11273–11279.
23. Hertz L, Peng L, Dienel GA (2007) Energy metabolism in astrocytes: High rate of oxidative metabolism and spatiotemporal dependence on glycolysis/glycogenolysis. *J Cereb Blood Flow Metab* 27(2):219–249.
24. Schwartz WJ, et al. (1979) Metabolic mapping of functional activity in the hypothalamo-neurohypophysial system of the rat. *Science* 205(4407):723–725.
25. Mata M, et al. (1980) Activity-dependent energy metabolism in rat posterior pituitary primarily reflects sodium pump activity. *J Neurochem* 34(1):213–215.
26. Attwell D, Laughlin SB (2001) An energy budget for signaling in the grey matter of the brain. *J Cereb Blood Flow Metab* 21(10):1133–1145.
27. Hall CN, Klein-Flügge MC, Howarth C, Attwell D (2012) Oxidative phosphorylation, not glycolysis, powers presynaptic and postsynaptic mechanisms underlying brain information processing. *J Neurosci* 32(26):8940–8951.
28. Cohen DM, et al. (2002) A method for measuring cerebral glucose metabolism in vivo by ^{13}C-NMR spectroscopy. *Magn Reson Med* 48(6):1063–1067.
29. Deuel RK, Yue GM, Sherman WR, Schickner DJ, Ackerman JJ (1985) Monitoring the time course of cerebral deoxyglucose metabolism by ^{31}P nuclear magnetic resonance spectroscopy. *Science* 228(4705):1329–1331.
30. Chapman AG, Meldrum BS, Siesjö BK (1977) Cerebral metabolic changes during prolonged epileptic seizures in rats. *J Neurochem* 28(5):1025–1035.
31. Nakanishi H, Cruz NF, Adachi K, Sokoloff L, Dienel GA (1996) Influence of glucose supply and demand on determination of brain glucose content with labeled methylglucose. *J Cereb Blood Flow Metab* 16(3):439–449.
32. Tokugawa J, Ravasi L, Nakayama T, Schmidt KC, Sokoloff L (2007) Operational lumped constant for FDG in normal adult male rats. *J Nucl Med* 48(1):94–99.
33. Henn FA, Anderson DJ, Rustad DG (1976) Glial contamination of synaptosomal fractions. *Brain Res* 101(2):341–344.
34. Choi IY, Lei H, Gruetter R (2002) Effect of deep pentobarbital anesthesia on neurotransmitter metabolism in vivo: On the correlation of total glucose consumption with glutamatergic action. *J Cereb Blood Flow Metab* 22(11):1343–1351.
35. Duarte JM, Lanz B, Gruetter R (2011) Compartmentalized cerebral metabolism of [1,6-^{13}C]glucose determined by in vivo ^{13}C NMR spectroscopy at 14.1 T. *Front Neuroenergetics* 3:3.
36. Dienel GA, Schmidt KC, Cruz NF (2007) Astrocyte activation in vivo during graded photic stimulation. *J Neurochem* 103(4):1506–1522.
37. Ikemoto A, Bole DG, Ueda T (2003) Glycolysis and glutamate accumulation into synaptic vesicles. Role of glyceraldehyde phosphate dehydrogenase and 3-phosphoglycerate kinase. *J Biol Chem* 278(8):5929–5940.
38. Ishida A, Noda Y, Ueda T (2009) Synaptic vesicle-bound pyruvate kinase can support vesicular glutamate uptake. *Neurochem Res* 34(5):807–818.
39. Hertz L, Yu AC, Kala G, Schousboe A (2000) Neuronal-astrocytic and cytosolic-mitochondrial metabolite trafficking during brain activation, hyperammonemia and energy deprivation. *Neurochem Int* 37(2-3):83–102.
40. Palaiologos G, Hertz L, Schousboe A (1988) Evidence that aspartate aminotransferase activity and ketodicarboxylate carrier function are essential for biosynthesis of transmitter glutamate. *J Neurochem* 51(1):317–320.
41. Caesar K, et al. (2008) Glutamate receptor-dependent increments in lactate, glucose and oxygen metabolism evoked in rat cerebellum in vivo. *J Physiol* 586(5):1337–1349.
42. Nehlig A, Wittendorp-Rechenmann E, Lam CD (2004) Selective uptake of [^{14}C]2-deoxyglucose by neurons and astrocytes: High-resolution microautoradiographic imaging by cellular ^{14}C-trajectography combined with immunohistochemistry. *J Cereb Blood Flow Metab* 24(9):1004–1014.
43. Itoh Y, Abe T, Takaoka R, Tanahashi N (2004) Fluorometric determination of glucose utilization in neurons in vitro and in vivo. *J Cereb Blood Flow Metab* 24(9):993–1003.
44. Barros LF, et al. (2009) Preferential transport and metabolism of glucose in Bergmann glia over Purkinje cells: A multiphoton study of cerebellar slices. *Glia* 57(9): 962–970.
45. Jakoby P, et al. (2014) Higher transport and metabolism of glucose in astrocytes compared with neurons: A multiphoton study of hippocampal and cerebellar tissue slices. *Cereb Cortex* 24(1):222–231.
46. Chowdhury GM, Patel AB, Mason GF, Rothman DL, Behar KL (2007) Glutamatergic and GABAergic neurotransmitter cycling and energy metabolism in rat cerebral cortex during postnatal development. *J Cereb Blood Flow Metab* 27(12):1895–1907.
47. Badar-Goffer RS, Ben-Yoseph O, Bachelard HS, Morris PG (1992) Neuronal-glial metabolism under depolarizing conditions. A ^{13}C-n.m.r. study. *Biochem J* 282(Pt 1): 225–230.
48. Occhipinti R, Somersalo E, Calvetti D (2009) Astrocytes as the glucose shunt for glutamatergic neurons at high activity: An in silico study. *J Neurophysiol* 101(5):2528–2538.
49. Bolaños JP, Almeida A, Moncada S (2010) Glycolysis: A bioenergetic or a survival pathway? *Trends Biochem Sci* 35(3):145–149.
50. Shetty PK, Sadgrove MP, Galeffi F, Turner DA (2012) Pyruvate incubation enhances glycogen stores and sustains neuronal function during subsequent glucose deprivation. *Neurobiol Dis* 45(1):177–187.
51. Dienel GA, Ball KK, Cruz NF (2007) A glycogen phosphorylase inhibitor selectively enhances local rates of glucose utilization in brain during sensory stimulation of conscious rats: Implications for glycogen turnover. *J Neurochem* 102(2):466–478.
52. Mangia S, Simpson IA, Vannucci SJ, Carruthers A (2009) The in vivo neuron-to-astrocyte lactate shuttle in human brain: Evidence from modeling of measured lactate levels during visual stimulation. *J Neurochem* 109(Suppl 1):55–62.
53. Bélanger M, Allaman I, Magistretti PJ (2011) Brain energy metabolism: Focus on astrocyte-neuron metabolic cooperation. *Cell Metab* 14(6):724–738.
54. Lai JCK, Clark JB (1989) *Isolation and Characterization of Synaptic and Nonsynaptic Mitochondria From Mammalian Brain* (Humana Press, Inc., Clifton, NJ).
55. Patel AB, et al. (2005) Cerebral pyruvate carboxylase flux is unaltered during bicuculline-seizures. *J Neurosci Res* 79(1-2):128–138.